nature physics

LETTERS

https://doi.org/10.1038/s41567-017-0011-x

Coherent inflationary dynamics for Bose–Einstein condensates crossing a quantum critical point

Lei Feng, Logan W. Clark, Anita Gaj and Cheng Chin*

Quantum phase transitions, transitions between many-body ground states, are of extensive interest in research ranging from condensed-matter physics to cosmology[1–4]. Key features of the phase transitions include a stage with rapidly growing new order, called inflation in cosmology[5], followed by the formation of topological defects[6–8]. How inflation is initiated and evolves into topological defects remains a hot topic of debate. Ultracold atomic gas offers a pristine and tunable platform to investigate quantum critical dynamics[9–21]. We report the observation of coherent inflationary dynamics across a quantum critical point in driven Bose–Einstein condensates. The inflation manifests in the exponential growth of density waves and populations in well-resolved momentum states. After the inflation stage, extended coherent dynamics is evident in both real and momentum space. We present an intuitive description of the quantum critical dynamics in our system and demonstrate the essential role of phase fluctuations in the formation of topological defects.

During a quantum phase transition, a many-body system, originally prepared in the ground state with macroscopic coherence, is suddenly transferred to a metastable state after passing the critical point[1,6,12]. An example shown in Fig. 1 is a ferromagnetic transition where the Z_2 inversion symmetry is broken. How does the system evolve toward the new ground states generally with a different symmetry? One can hypothesize two possible scenarios. In the first scenario, fluctuations break the system into locally coherent segments that evolve toward the new ground states independently. After relaxation, the system forms domains with local coherence[2,12]. In the second scenario, although the macroscopic coherence is maintained, the system undergoes a coherent population transfer of particles toward lower energy states. Here fluctuations determine the domain structure but do not destroy the macroscopic coherence.While both scenarios support rapid evolution toward new ground states, the key differences are the time and length scales of the coherence in the dynamical process.

In this paper, we report the observation of coherent inflationary dynamics in an atomic Bose condensate driven across a quantum critical point. Our experiment is based on caesium Bose–Einstein condensates loaded into a one-dimensional phase-modulated optical lattice[22]. The modulation translates the lattice periodically over time t with displacement $\Delta x = \frac{s}{2}\sin\omega t$, where s is the shaking amplitude and ω is the shaking frequency. Shaking hybridizes the ground and excited Bloch bands and results in an effective dispersion ε_q for the condensate[22], where the lowest energy state at quasi-momentum $q=0$ bifurcates into two ground states at $+q^*$ and $-q^*$ (named pseudo-spin up and down), when s exceeds a critical value s_c. When the system is driven across the critical point in finite time, domains of pseudo-spins form in accordance with universal Kibble–Zurek scaling[21] and excitations within a domain display a roton dispersion[23]; however, a complete understanding of the processes that underlie the quantum critical dynamics remains evasive.

To reveal the nature of the quantum phase transition, we exploit three schemes to analyse the critical dynamics of the condensate: in situ imaging to record the atomic density profile; time-of-flight with a focusing technique[24] to probe the momentum space distribution n_q; and pseudo-spin reconstruction to reveal domain structure[21]. An example is shown in Fig. 2. Here we linearly ramp up the shaking amplitude and interrupt the ramp at time t after passing the critical point to probe the system with the three methods.

We observe two key features indicating coherent evolution. First, from in situ images, a density wave emerges about 20 ms after passing the critical point. Quantified with the density structure factor S_q (ref. [25]), the density wave shows an almost fixed wavenumber. Second, from time-of-flight images, the atomic population forms sharp side peaks in individual samples; over repeated measurements, the side peaks average to broader features. These observations suggest that atoms occupy a coherent superposition of well-defined momentum states and the density wave emerges from their interference. Although the density wave diminishes after 30 ms, the persistent narrow momentum peaks in atomic population n_q suggest a long-lasting coherence. In addition, the period of the density waves approximately matches twice the averaged domain size. Both features will be further discussed in later paragraphs.

A more comprehensive analysis of the density wave and the population distribution in momentum space suggests that the system evolution can be separated into two stages: inflation and relaxation. To see this, we evaluate the density variance $\delta n^2 = \int \mathrm{d}q S_q$ from in situ images as well as the total population in finite momentum states $\Delta N = \sum_{q>0} N_q$ from time-of-flight measurements, where N_q is the total atom number in the $\pm q$ states. For short times after the phase transition, both quantities show a characteristic exponential-like growth; we name this period the inflation stage (see Fig. 2f). After inflation, all atoms relax toward non-zero momentum states at $q=\pm q^*$ while the density wave diminishes. In the following, we investigate the two stages separately.

The exponential growth of excitations can be theoretically understood on the basis of dynamical instability of the condensate[26]. Shortly after passing the quantum critical point, the $q=0$ state remains macroscopicly occupied, which justifies the Bogliubov approximation. Owing to the inverted dispersion, the many-body Hamiltonian cannot be diagonalized with bosonic field operators[27]. Instead, we can write the Hamiltonian as (Supplementary Information)

$$H = \sum_{q>0} \hbar\lambda_q \left(\hat{\imath}_q^\dagger \hat{\imath}_{-q}^\dagger + \hat{\imath}_q \hat{\imath}_{-q} \right) \tag{1}$$

The James Franck Institute, Enrico Fermi Institute and Department of Physics, University of Chicago, Chicago, IL, USA. *e-mail: cchin@uchicago.edu

© 2017 Macmillan Publishers Limited, part of Springer Nature. All rights reserved.

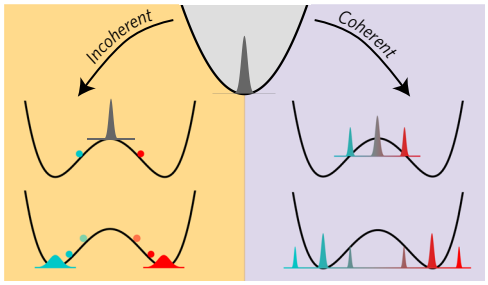

Fig. 1 | Paradigms of dynamics crossing a ferromagnetic quantum critical point. Two scenarios describing the quantum phase transition. Left, in the incoherent picture, the system is broken into locally coherent segments by fluctuations. Each segment evolves independently toward a new ground state. Particles eventually rethermalize at the energy minima to form domains. Right, in the coherent scenario, the system evolves toward the new ground states with macroscopic coherence extending beyond the domain size.

where $\hat{t}_q^\dagger$ and $\hat{t}_q$ are the bosonic creation and annihilation operators of an inflaton with momentum q and growth rate $\lambda_q = \sqrt{-\varepsilon_q(2\mu+\varepsilon_q)}/\hbar$, μ is the chemical potential and $\hbar$ is the reduced Planck constant. It is important to emphasize that only modes with negative kinetic energy $\varepsilon_q < 0$ acquire the inflationary dynamics. According to the Hamiltonian, the excited populations increase exponentially in the inflation phase according to (Supplementary Information)

$$N_q(t) + 1 = [N_q(0) + 1]\cosh 2\lambda_q t \quad (2)$$

and the structure factor $S_q(t) = (-\varepsilon_q/\mu)[N_q(t)+1]$ near the critical point. This result explains the similar exponential-like growth of both observables in Fig. 2f.

To further test the inflation theory, we perform quench experiments by suddenly driving the system across the critical point, and measure the growth rate of the population in different momentum modes. Right before the quench, we seed a small initial population in the desired momentum states $\pm q'$ by imprinting a sinusoidal phase pattern on the condensate $\delta\phi \sin(q'x/\hbar)$. Here $\delta\phi$ is the seed amplitude and the wavenumber $q'/\hbar$ is externally controlled (see Methods).

After seeding, the condensate quickly grows two side peaks at the seeding momentum $\pm q'$ (Fig. 3a). To extract the growth rate, we monitor the population in the momentum states. The population grows exponentially in the beginning but reaches a maximum at a later time when the population in the $k = 0$ state is depleted (Fig. 3b). We fit the fast-growing interval right after the quench according to equation (2) and compare the growth rate to the prediction (Fig. 3c). Our measured growth rates qualitatively agree with the Bogoliubov result. We find quantitative agreement with our numerical simulation based on

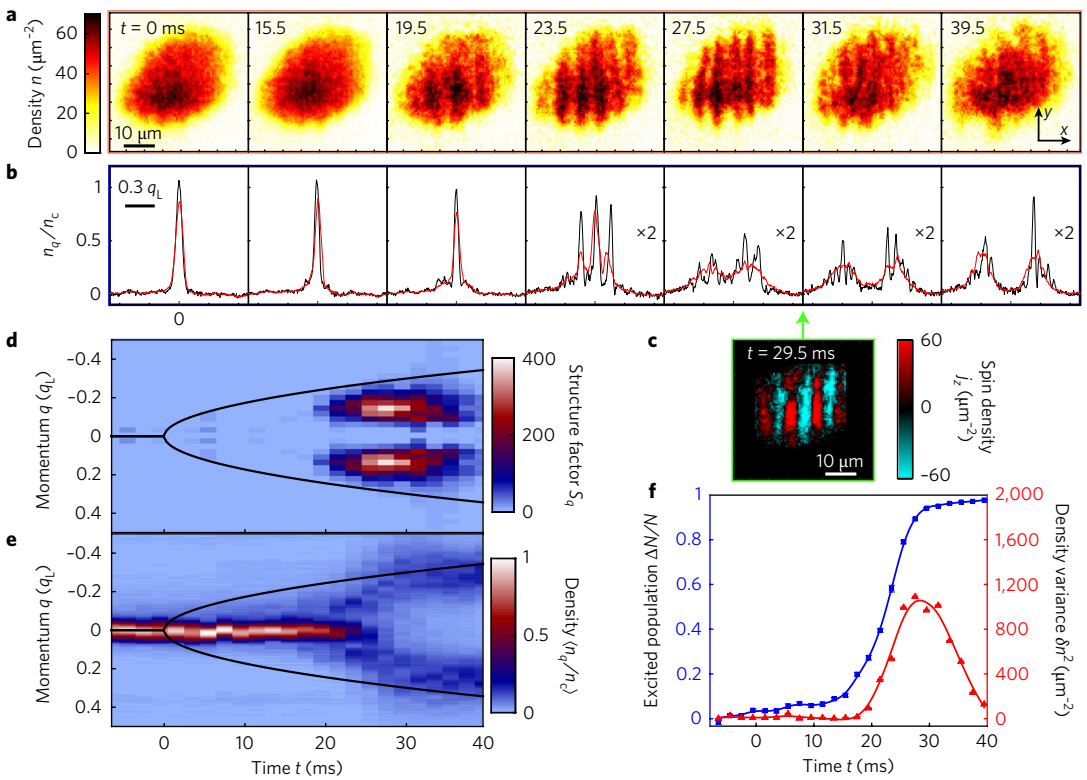

Fig. 2 | Development of density waves and momentum space population across the quantum critical point. Density waves and sharp peaks in momentum space emerge when we linearly ramp up the shaking amplitude s with a ramp rate $\dot{s} = 0.64\,\mathrm{nm\,ms^{-1}}$ across the critical point $s_c = 13.1\,\mathrm{nm}$ at time $t = 0$. **a**, Single-shot in situ images of the condensate. **b**, Momentum distribution n_q from time-of-flight measurement (black). Here n_c is the averaged peak density in the momentum space of unshaken condensates. Averaging over repeated experiments gives two broad peaks centred around $q = 0$ (red). **c**, Domain structure from reconstruction[21], where $j_z = n_{q^*} - n_{-q^*}$ is the spin density. **d**, The density structure factor $S_q = \langle \Delta n_q^2 \rangle / N$, extracted from the Fourier transform of the density fluctuation $\Delta n(x) = n(x) - \langle n(x) \rangle$ integrated along the y axis. Here N is the total atom number and $\langle\ .\ \rangle$ indicates an average over repeated measurements. Peaks appear at $\pm q_d = \pm 0.14\ q_L$, with $q_L = \pi\hbar/d$ being the lattice momentum and d being the lattice period. **e**, The averaged population distribution $\langle n_q \rangle$ in momentum space. The solid black curves in **d** and **e** show the instantaneous, theoretical ground-state momenta $\pm q^*$. **f**, Fractional population excited out of q=0 state (blue squares) and the density variance δn^2 from integrating the structure factor S_q. The solid lines are guides to the eye. The error bars indicate 1σ standard error.

© 2017 Macmillan Publishers Limited, part of Springer Nature. All rights reserved.

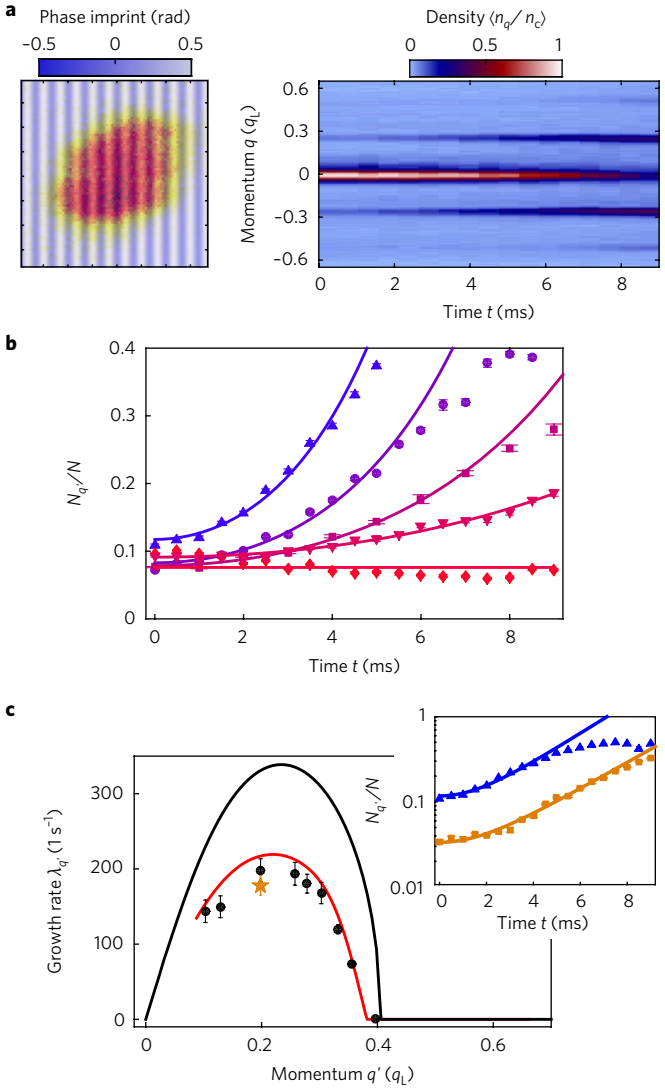

Fig. 3 | Growth of excitations during the inflation phase. We quench the seeded condensates from shaking amplitude s_c=13.1 nm to s=25 nm, where the new ground states are at $\pm q^* = \pm 0.24\ q_L$. **a**, At $t = 0$, we quickly imprint a phase modulation in 20 μs on the condensate with a seeding momentum $q' = 0.26\ q_L$ (left). Subsequent time-of-flight measurements reveal two side peaks emerging at $\pm q'$ (right). **b**, The fractional population in both side peaks $N_{q'}/N$ evolves for different seeding momentum: $q' = 0.19$ (triangles), 0.30 (circles), 0.33 (squares), 0.36 (inverted triangles) and 0.40 q_L (diamonds), from blue to red. The solid lines are fits using equation (2) to extract the growth rate $\lambda_{q'}$. **c**, The growth rates for seeded (black) and unseeded experiments (orange star) are compared with Bogoliubov theory (black line) and numerical simulation (red line). The inset shows a comparison of the growth for the seeded experiment with $q' = 0.19\ q_L$ (blue) and the unseeded quench experiment (orange). The error bars indicate 1σ standard error.

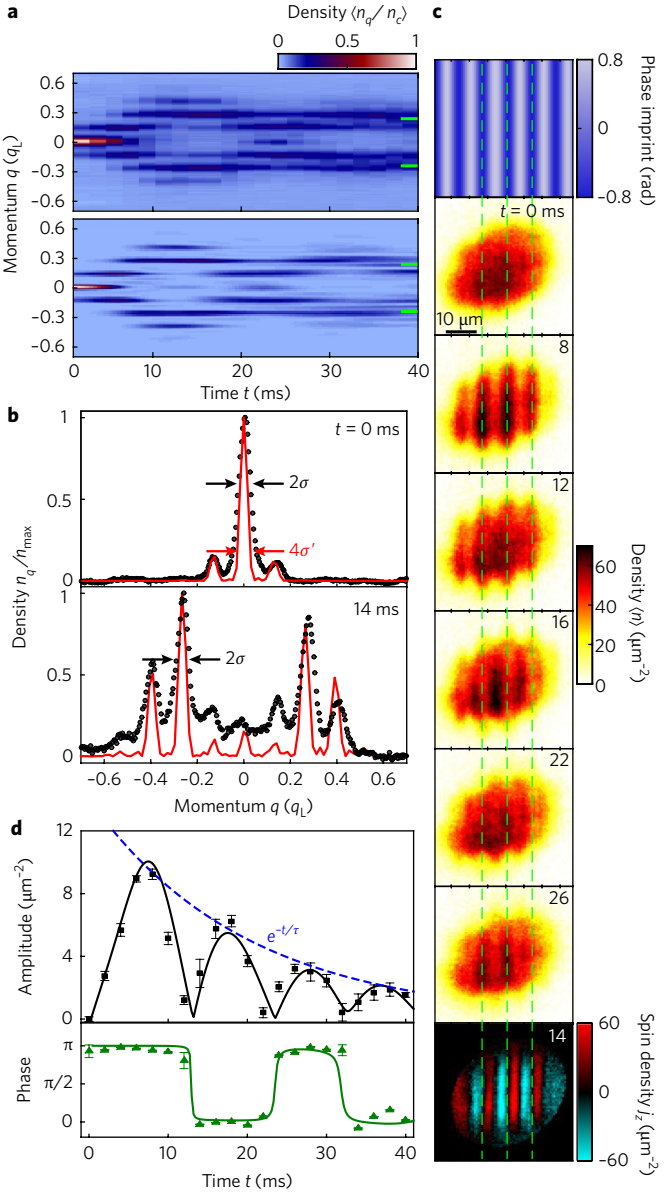

Fig. 4 | Coherent quantum critical dynamics. The condensates are seeded at momentum $q' = 0.13\ q_L$ and quenched from shaking amplitude s_c=13.1 nm to s= 25 nm. **a**, Coherent oscillations in momentum space (top: experiment; bottom: numerical calculation). The green solid lines indicate the position of $\pm q^*$. **b**, Line cuts of the experimental data at $t = 0$ and 14 ms (black dot). The solid red lines are from numerical calculations. The experimental peaks in both cuts show similar root-mean-square radii of $\sigma = 0.026\ q_L$ and $0.028\ q_L$ from Gaussian fits. The numerical calculation shows $\sigma' = 0.015\ q_L$, determined by the sample size. **c**, Oscillation of the density wave and the domain structure at $t = 14$ ms. Both density waves and domains appear aligned with the seed pattern (green dashed line). **d**, Amplitude (black squares) and phase (green triangles) of the density wave are compared with the numerical calculation (solid lines). A settling time $\tau = 20$ ms is extracted from the decay of the envelope function (blue dashed line). The error bars indicate 1σ standard error.

the Gross–Piteavskii equation that incorporates the depletion of the condensate (Supplementary Information). In particular, we confirm that only modes $|q| \leq 0.4\ q_L$ with kinetic energy $\varepsilon_q < 0$ exponentially grow and the fastest growth appears at momentum $q \approx \pm q^*$. Here $q_L = \pi\hbar/d$ is the lattice momentum with d being the lattice period.

Remarkably, in the absence of seeding, the sample spontaneously grows momentum peaks near $\pm q^*$ with a growth rate very close to that seeded at a similar momentum (Fig. 3c and the inset). For unseeded samples, many momentum modes can, in principle, be populated by quantum or thermal fluctuations and then amplified by inflation. The dominance of the modes near $\pm q^*$ can be understood since they have the highest growth rate and become dominant during inflation.

Following the inflation stage, the condensates display persistent coherent dynamics in both time-of-flight and in situ measurements (Fig. 4). After the rapid growth of the population at seeded momentum

© 2017 Macmillan Publishers Limited, part of Springer Nature. All rights reserved.

$\pm q'$, the system generates higher order harmonics at $\pm 2q', \pm 3q' \ldots$, and the atomic populations are coherently′ transferred between these momentum states. The emergence of higher harmonics is due to nonlinear mixing of the matter waves and can be well described based on our numerical model. An example at $t = 14$ ms shows multiple side peaks that conform to the simulation. Intriguingly, the individual momentum peaks are as narrow as the zero momentum peak of the original condensate; the widths are limited only by the detection resolution. A narrow momentum peak indicates long coherence length based on uncertainty principle. By comparing our measurement with the simulation, we conclude that the lower bound of the coherence length is 15 μm, which is much greater than the average domain size of 4.1(1) μm (Supplementary Information).

Together with the dynamics in momentum space, density waves in seeded samples also display coherent oscillations in quench experiments (Fig. 4c). The density wave appears aligned to the imprinted pattern, and its phase displays multiple alternations (Fig. 4d) that are synchronized with oscillations of the population in momentum space. The contrast of the density wave oscillates and slowly decays with a time constant of $\tau = 20$ ms. Both the alternation and the decay are in good agreement with our simulation. Finally, we find that domains are fully formed as early as $t = 14$ ms, and remain constant afterward. Importantly, the domain structure is deterministic in the seeded experiments, and the domain walls line up with the density wave yielding a domain size half the period of the density wave.

The observed coherent dynamics can be understood on the basis of a simple physical picture. Phase imprinting across the condensate locally breaks the inversion symmetry by inserting a current $j = \frac{\hbar}{m}\phi'(x)$, where $\phi(x)$ is the phase of the condensate wavefunction. Within one period of the imprinted phase pattern, the sign of the local momentum flips twice, resulting in two neighbouring domains with opposite momenta. After the momentum kick, atoms in neighboring domains can flow toward or away from each other determined by the group velocity $v_g(x) = \mathrm{d}\varepsilon_q/\mathrm{d}q$, leading to the observed density peaks and troughs. Since density waves cost energy in a Bose–Einstein condensate with repulsive interactions, the atom flow reverses after half an oscillation period, yielding the phase alternation of the density wave.

The decisive role of phase imprinting in the real- and momentum-space dynamics and domain structure indicates the importance of phase fluctuations in quantum critical dynamics. In addition to the emergence of density waves and atomic occupation in well-resolved momentum states, we present strong evidence supporting the coherent scenario of the quantum phase transition in our system. Furthermore, the phase imprinting technique can find new applications in engineering desired structures of domain walls, which will enable future study on the dynamics and interactions of topological defects.

Methods

Methods, including statements of data availability and any associated accession codes and references, are available at https://doi.org/10.1038/s41567-017-0011-x.

Received: 16 June 2017; Accepted: 10 October 2017;
Published online: 18 December 2017

References

1. Sachdev, S. *Quantum Phase Transitions* 1st edn (Cambridge Univ. Press, Cambridge, 2011).
2. Morikawa, M. Cosmological inflation as a quantum phase transition. *Progr. Theoret. Phys.* **93**, 685–709 (1995).
3. Kibble, T. W. B. Some implications of a cosmological phase transition. *Phys. Rep.* **67**, 183–199 (1980).
4. Vojta, T. Quantum phase transitions. *AIP Conf. Proc.* **1550**, 288–247 (2013).
5. Guth, A. H. Inflationary universe: A possible solution to the horizon and flatness problems. *Phys. Rev. D* **23**, 347–356 (1981).
6. Kibble, T. W. B. Topology of cosmic domains and strings. *J. Phys. A* **9**, 1387–1398 (1976).
7. Zurek, H. W. Cosmological experiments in superfluid helium? *Nature* **317**, 505–508 (1985).
8. del Campo, A. & Zurek, W. H. Universality of phase transition dynamics: Topological defects from symmetry breaking. *Int. J. Mod. Phys. A* **29**, 1430018 (2014).
9. Sadler, L. E., Higbie, J. M., Leslie, S. R., Vengalattore, M. & Stamper-Kurn, D. M. Spontaneous symmetry breaking in a quenched ferromagnetic spinor Bose–Einstein condensate. *Nature* **443**, 312–315 (2006).
10. Polkovnikov, A., Sengupta, K., Silva, A. & Vengalattore, M. Nonequilibrium dynamics of closed interacting quantum systems. *Rev. Mod. Phys.* **83**, 863–883 (2011).
11. Bloch, I., Dalibard, J. & Zwerger, W. Many-body physics with ultracold gases. *Rev. Mod. Phys.* **80**, 885–964 (2008).
12. Dziarmaga, J. Dynamics of a quantum phase transition and relaxation to a steady state. *Adv. Phys.* **59**, 1063–1189 (2010).
13. Baumann, K., Mottl, R., Brennecke, F. & Esslinger, T. Exploring symmetry breaking at the Dicke quantum phase transition. *Phys. Rev. Lett.* **107**, 140402 (2011).
14. Barnett, R., Polkovnikov, A. & Vengalattore, M. Prethermalization in quenched spinor condensates. *Phys. Rev. A* **84**, 023606 (2011).
15. Lamporesi, G., Donadello, S., Serafini, S., Dalfovo, F. & Ferrari, G. Spontaneous creation of Kibble–Zurek solitons in a Bose–Einstein condensate. *Nat. Phys.* **9**, 656–660 (2013).
16. Nicklas, E. et al. Observation of scaling in the dynamics of a strongly quenched quantum gas. *Phys. Rev. Lett.* **115**, 245301 (2015).
17. Navon, N., Gaunt, A. L., Smith, R. P. & Hadzibabic, Z. Critical dynamics of spontaneous symmetry breaking in a homogeneous Bose gas. *Science* **347**, 167–170 (2015).
18. Klinder, J., Keler, H., Wolke, M., Mathey, L. & Hemmerich, A. Dynamical phase transition in the open Dicke model. *Proc. Natl Acad. Sci. USA* **112**, 3290–3295 (2015).
19. Meldgin, C. et al. Probing the Bose glass–superfluid transition using quantum quenches of disorder. *Nat. Phys.* **12**, 646–649 (2016).
20. Anquez, M. et al. Quantum Kibble–Zurek mechanism in a spin-1 Bose–Einstein condensate. *Phys. Rev. Lett.* **116**, 155301 (2016).
21. Clark, L. W., Feng, L. & Chin, C. Universal space-time scaling symmetry in the dynamics of bosons across a quantum phase transition. *Science* **354**, 606–610 (2016).
22. Parker, C. V., Ha, L.-C. & Chin, C. Direct observation of effective ferromagnetic domains of cold atoms in a shaken optical lattice. *Nat. Phys.* **9**, 769–774 (2013).
23. Ha, L.-C., Clark, L. W., Parker, C. V., Anderson, B. M. & Chin, C. Roton-maxon excitation spectrum of bose condensates in a shaken optical lattice. *Phys. Rev. Lett.* **114**, 055301 (2015).
24. Shvarchuck, I. et al. Bose–Einstein condensation into nonequilibrium states studied by condensate focusing. *Phys. Rev. Lett.* **89**, 270404 (2002).
25. Hung, C. L. et al. Extracting density–density correlations from in situ images of atomic quantum gases. *Phys. Rev. A* **59**, 4595–4607 (1999).
26. Morsch, O. & Oberthaler, M. Dynamics of Bose–Einstein condensates in optical lattices. *Rev. Mod. Phys.* **78**, 179–215 (2006).
27. Anglin, J. R. Second-quantized Landau–Zener theory for dynamical instabilities. *Phys. Rev. A* **67**, 051601 (2003).

Acknowledgements

We thank E. Berg, Q. Zhou and B. M. Anderson for helpful discussions. L.W.C. was supported by a Grainger fellowship. A.G. is supported by a Kadanoff–Rice fellowship. This work was supported by the University of Chicago Materials Research Science and Engineering Center, which is funded by the National Science Foundation under award number DMR-1420709, NSF grant PHY-1511696 and Army Research Office-Multidisciplinary Research Initiative grant W911NF-14-1-0003.

Author contributions

L.F. and L.W.C. designed the experiments. L.F. performed the experiments and analysed the data. L.F. and C.C. prepared the manuscript. All authors contributed discussions on experiments and the manuscript. C.C. supervised.

Competing interests

The authors declare no competing financial interests.

Additional information

Supplementary information is available for this paper at https://doi.org/10.1038/s41567-017-0011-x.

Reprints and permissions information is available at www.nature.com/reprints.

Correspondence and requests for materials should be addressed to C.C.

Publisher's note: Springer Nature remains neutral with regard to jurisdictional claims in published maps and institutional affiliations.

© 2017 Macmillan Publishers Limited, part of Springer Nature. All rights reserved.

Methods

Lattice loading. We utilize three-dimensional Bose–Einstein condensates of 30,000 caesium atoms confined in an optical dipole trap. The trap is tightly confined in the gravity direction with a trapping frequency of $2\pi\times226$ Hz. Trapping frequencies in the two in-plane directions are $2\pi\times6$ and $2\pi\times9$ Hz. The *s*-wave scattering length is 2.6 nm. We adiabatically load the Bose–Einstein condensate into a one-dimensional optical lattice with a depth of 8.9 E_R and period $d=532$ nm, where $E_R=h\times 1.3$ kHz is the recoil energy.

Shaken lattice. We periodically translate the lattice by sinusoidally modulating the phase of one of the lattice beams. The shaking frequency is fixed to $\omega=2\pi\times8$ kHz, which is $2\pi\times0.87$ kHz above the gap at zero momentum between the ground and the first excited Bloch band in the lattice.

Phase imprinting. We imprint the phase pattern across the condensate using a digital micromirror device with a 795 nm laser. To ensure a sinusoidal modulation, we set a grating pattern on the digital micromirror device with twice the desired period $2\pi\hbar/q'$ and let only the ±1 orders from the diffraction pass in the Fourier plane. The diffracted beams interfere on the atoms, giving a clean sinusoidally varying potential. The imprinting pulse lasts for 20 to 40 μs, which is very short compared with the condensate and lattice timescale.

Data availability. The data that support the plots within this paper and other findings of this study are available from the corresponding author upon reasonable request.

© 2017 Macmillan Publishers Limited, part of Springer Nature. All rights reserved.